Inorganic Chemistry

Article

pubs.acs.org/IC

# $Ba_{13}Si_6Sn_8As_{22}$: A Quaternary Zintl Phase Containing Adamantane-Like $[Si_4As_{10}]$ Clusters

Xiao-Cun Liu, Na Lin, Jian Wang, Ming-Yan Pan, Xian Zhao, Xu-Tang Tao, and Sheng-Qing Xia*

State Key Laboratory of Crystal Materials, Institute of Crystal Materials, Shandong University, Jinan, Shandong 250100, People's Republic of China

Supporting Information

**ABSTRACT:** A new quaternary arsenide Zintl phase, $Ba_{13}Si_6Sn_8As_{22}$, has been synthesized from the Sn-flux reactions, and the structure was determined by the single-crystal X-ray diffraction methods. The compound crystallizes in the tetragonal non-centrosymmetric space group $I\bar{4}2m$ (No. 121) with unit cell parameters of $a = b =$ 14.4857(3) Å, $c =$ 13.5506(7) Å, $V =$ 2843.40(17) Å$^3$. Its polyanion structure can be viewed as composed of $[Si_4As_{10}]$ adamantane-like clusters and $SiAs_4$ tetrahedra, which are linked via the $[Sn_2As_4]$ groups built through two edge-sharing $SnAs_3$ triangular pyramids. Differential thermal analysis and thermogravimetry measurements indicate that $Ba_{13}Si_6Sn_8As_{22}$ has good thermal stability, and does not melt or decompose below 1045 K under Ar atmosphere. Density functional calculations were performed on $Ba_{13}Si_6Sn_8As_{22}$ and the results suggest a band gap of around 1.0 eV for $Ba_{13}Si_6Sn_8As_{22}$, confirmed by the diffuse reflectance spectrum measurement. In addition, the extensively existing lone pairs of electrons on the *p*-orbitals of As and Sn may also hint interesting nonlinear optical properties considering the noncentrosymmetric structure.

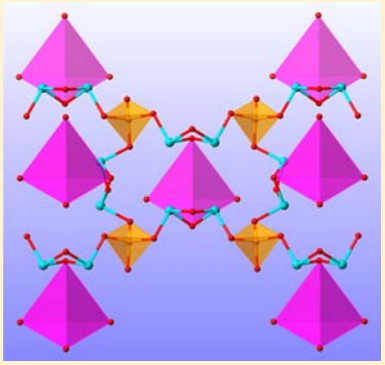

## INTRODUCTION

Pnictide-based Zintl phases are of interest due to their diverse crystal structures and unusual electronic structures.[1−5] In the past decade, abundant physical properties such as semiconducting,[6] superconducting,[7−9] colossal magnetoresistance,[10] and thermoelectricity[11−14] have been frequently reported for such polar intermetallic phases. For example, high superconducting transition temperature has been discovered in $ThCr_2Si_2$-type $AFe_2As_2$ (A = K, Rb, Cs, Sr, Ba) and PbFCl-type AFeAs (A = Li, Na) series and related studies were immediately undertaken all over the world.[8,9] Besides, with more and more new pnictide-based Zintl compounds discovered and explored recently, studies involving their crystal and electronic structures have become a research focus in related fields.[15−19]

Semiconducting compounds with the noncentrosymmetric structural arrangement are critical in developing new materials for nonlinear optical (NLO) applications.[20] Our previous exploration on the cadmium-pnictide-based system $A_2CdPn_2$ (*A* = Ca, Sr, Ba, Eu; *Pn* = P or As) has led to the discovery of a series of new Zintl compounds with noncentrosymmetric structures and interesting polymorphisms.[21] The studies prompted us to extend the system to contain the tetrels, and a new arsenide-based Zintl compound, $Ba_{13}Si_6Sn_8As_{22}$, was accidentally obtained. The compound features a new noncentrosymmetric structure type containing the adamantane-like $[Si_4As_{10}]$ clusters. Interestingly, a recent report indicated that strong SHG effects could originate from similar adamantane-like units, i.e., $Ba_3CsGa_5Se_{10}Cl_2$ with its overall polarity predominantly contributed by the $[Ga_4Se_{10}]$ supertetrahedra.[22] It should be noted that such adamantane-like clusters were usually seen in chalcogenide-based complexes such as $K_4Si_4Te_{10}$,[23] $RbInQ_2$ (Q = S, Se),[24] $NaAlSe_2$,[25] and $KInS_2$.[26] For Pnictide-based Zintl phases, examples containing adamantane-like clusters are relatively few: a rare analogue is $Na_2SnAs_2$, which features different $[Sn_4As_{10}]$ clusters and was reported about twenty years ago.[27]

In this paper, we presented the flux synthesis of a new quaternary arsenide Zintl compound, $Ba_{13}Si_6Sn_8As_{22}$, for which the structure was accurately determined by using single-crystal X-ray diffraction methods. The structure of this compound features diverse polyanion units and unusual cation coordination geometries, which exhibits abundant crystal chemistry information and is worthy of in-depth studies. Density functional theoretical calculations were also incorporated to study the electronic structure and the results indicated an indirect band gap, supported by the measured diffuse reflectance spectrum. Related thermal stability studies were provided with the aid of differential thermal analysis and thermogravimetry measurements as well.

## EXPERIMENTAL SECTION

**Synthesis.** All syntheses were performed in an argon-filled glovebox with the oxygen level below 0.1 ppm or under vacuum. The elements were commercially purchased and used as received: Ba (Afla, 99%), Si (Alfa, 99.999%), Sn (Alfa, 99.9%), As (Alfa, 99.999%). $Ba_{13}Si_6Sn_8As_{22}$ was initially synthesized from a Sn-flux reaction with a loading ratio of Ba:Si:Sn:As = 1:1:50:2 and the following procedure applied: the reactants were loaded in an alumina crucible which was

**Received:** May 25, 2013
**Published:** September 30, 2013

   dx.doi.org/10.1021/ic402023z | *Inorg. Chem.* 2013, 52, 11836−11842

subsequently sealed in an evacuated fused silica jacket; the container was then moved to a programmable furnace and the reactants were first heated to 1000 °C and homogenized at this temperature for 20 h, and then slowly cooled down to 400 °C at a rate of 5 °C/h. Finally the excessive flux was quickly decanted by centrifuge and the products consisted of a mixture of the title compound in block shape and the needle crystals of $Ba_3Sn_4As_6$.[28] After the crystal structure and composition of $Ba_{13}Si_6Sn_8As_{22}$ were accurately identified by single-crystal X-ray diffraction and EDX, the synthesis procedure was optimized in order to purify the product. A modified loading ratio of Ba:Si:Sn:As = 1:3:50:2, as well as the use of the higher reacting temperature (1100 °C) and flux removal temperature (600 °C), proved to best reproduce the target compound in high yield. The purity of the product was also confirmed by its powder X-ray diffraction patterns. The utilization of much excessive Si in the reaction can be explained if taking into account the poor solubility of Si in Sn-flux, and thus high Si-concentration can suppress the formation of the $Ba_3Sn_4As_6$ ternary phase. Stoichiometric reactions in Nb-tubes failed to reproduce the title compound, and the product was a mixture of some binary phases and $Ba_3Sn_4As_6$. $Ba_{13}Si_6Sn_8As_{22}$ is not sensitive to oxygen or moisture and the intensity of the powder diffraction patterns remains even after exposing the crystals in air for one week.

**Single Crystal X-ray Diffraction and Structure Determination.** Single crystals of $Ba_{13}Si_6Sn_8As_{22}$ were selected in the glovebox and cut in the Paratone-N oil. A crystal with suitable sizes (0.03 × 0.03 × 0.04 $mm^3$) was mounted on a glass fiber and collected on a Bruker CCD-based diffractometer at 296 K. Intensity data covering a full sphere of the reciprocal space were collected with four batch runs in $\omega$-scan mode. The frame width was 0.5° and the acquisition rate was 15 s per frame. Data reduction and integration, together with global unit cell refinements were done by the INTEGRATE program incorporated in the APEX2 software.[29] Semiempirical absorption corrections were applied using the SCALE program for area detector.[29]

The systematic absence of reflections with indexes $hkl$ ($h + k + l \neq 2n$); $0kl$ ($k + l \neq 2n$); $hk0$ ($h + k \neq 2n$); $h00$ ($h \neq 2n$); $hhl$ ($l \neq 2n$), and $00l$ ($l \neq 2n$) confirmed the body-centered tetragonal lattice and suggested several possible space groups: $I4$ (No. 79), $I\bar{4}$ (No. 82), $I4/m$ (No. 87), $I\bar{4}2m$ (No. 121), $I4/mmm$ (No. 139). The intensity statistics were consistent with the noncentrosymmetric symmetry, and the structure was solved in $I\bar{4}2m$ by direct methods and refined by full matrix least-squares methods on $F^2$ using SHELX.[30] The structure refinements with anisotropic thermal parameters quickly converged to small $R$ values ($R_1$ = 0.0196, $wR_2$ = 0.0444) and a reasonable Flack parameter of 0.014(17). However, the temperature parameters of Ba3 were very abnormal if compared with the other two barium cations. Refining this atom with freed occupation fraction resulted in an almost 100% occupancy, and the elemental analysis by EDX also suggested a composition in good agreement with the crystallographic data. These results excluded the possibility of the partially occupied site for Ba3. Thus, a difference Fourier map was plotted (Supporting Information) and the residual electron density around the Ba3 atom indicated a small split along the direction of Ba3−As5 bonds. Such a split could be understood by the special coordination environment of Ba3, which will be discussed below. Refining this position in the twofold split fashion was also tried and the corresponding anisotropic thermal parameters did improve (Table S1 in SI). However, since such a split is too small and the improvement is not very significant, an ordered model is still to be reported in this paper for the sake of concise structure description.

Crystallographic data and structural refinements are summarized in Table 1. Atomic positions and anisotropic displacement parameters are provided in Table 2. Selected bond lengths are given in Table 3. Further information in the form of CIF has been deposited with Fachinformationszentrum Karlsruhe, 76344 Eggenstein-Leopoldshafen, Germany, (fax: (49) 7247−808−666; e-mail: crysdata@fiz-karlsruhe.de) − depository CSD-number 426155.

**Powder X-ray Diffraction.** For phase identification, powder X-ray diffraction patterns were taken at room temperature by a Bruker AXS X-ray powder diffractometer using Cu−K$\alpha$ radiation. The data were recorded in a 2$\theta$ mode with a step size of 0.02° and a counting time of 10 s.

**Table 1. Selected Crystal Data and Structure Refinement Parameters for $Ba_{13}Si_6Sn_8As_{22}$**

| formula | $Ba_{13}Si_6Sn_8As_{22}$ |
|---|---|
| Fw/g·mol$^{-1}$ | 4551.72 |
| T/°C | 23(2) |
| Radiation, wavelength | Mo−K$\alpha$, 0.71073 Å |
| Space group, $Z$ | $I\bar{4}2m$ (No.121), 2 |
| Unit cell dimensions | |
| $a$/Å | 14.4857(3) |
| $c$/Å | 13.5506(7) |
| $V$/Å$^3$ | 2843.40(17) |
| $\rho_{calc}$/g·cm$^{-3}$ | 5.316 |
| $\mu_{Mo\ K\alpha}$/mm$^{-1}$ | 25.11 |
| Flack parameter | 0.014 (17) |
| Final $R$ indices[a] [$I > 2\sigma_{(I)}$] | $R_1$ = 0.0196 |
| | $wR_2$ = 0.0444 |
| Final $R$ indices[a] [all data] | $R_1$ = 0.0216 |
| | $wR_2$ = 0.0452 |

[a] $R_1 = \sum||F_o| - |F_c||/\sum|F_o|$; $wR_2 = [\sum[w(F_o^2 - F_c^2)^2]/\sum[w(F_o^2)^2]]^{1/2}$, and $w = 1/[\sigma^2F_o^2 + (A\cdot P)^2 + B\cdot P]$, $P = (F_o^2 + 2F_c^2)/3$; A and B are weight coefficients.

**Elemental Analysis.** Energy dispersive X-ray spectroscopy was taken on a picked single crystal of $Ba_{13}Si_6Sn_8As_{22}$ with a Hitachi FESEM-4800 field emission microscopy equipped with a Horiba EX-450 EDS. The measured composition matches well the results obtained from single-crystal X-ray diffraction data (Supporting Information).

**Differential Thermal Analysis and Thermogravimetry Measurements (DTA/TG).** The thermal stability of $Ba_{13}Si_6Sn_8As_{22}$ was tested using a Mettler-Toledo TGA/DSC/1600HT instrument. Thermogravimetric analysis (TGA) and differential scanning calorimetry (DSC) experiments were performed on a polycrystalline material sample (25.29 mg) under the protection of high-purity argon gas. A temperature range from 300 to 1070 K was applied with a heating rate of 10 K/min.

**UV−Vis−NIR Diffuse Reflectance Spectrum.** The diffuse reflectance spectrum of $Ba_{13}Si_6Sn_8As_{22}$ was measured on a polycrystalline sample at room temperature using a Shimadzu UV-3101 PC spectrometer equipped with an integrating sphere attachment and $BaSO_4$ as a reference. The absorption spectrum was calculated from the reflection spectrum *via* the Kubelka−Munk function: $\alpha/S = (1 - R)^2/2R$, in which $\alpha$ was the absorption coefficient, $S$ was the scattering coefficient, and $R$ was the reflectance.[31]

**Computational Details.** To better understand the structure relationship between this new phase and the closely related analogues, electronic band structure calculations were performed on $Ba_{13}Si_6Sn_8As_{22}$. The full potential linearized augmented plane wave method (FP-LAPW)[32,33] was applied with the aid of Wien2k code.[34] In this method, the unit cell is divided into nonoverlapping muffin-tin (MT) spheres and an interstitial region. The wave functions in the interstitial regions are expanded in plane waves up to $R_{MT} \times K_{max} = 7$, where $R_{MT}$ is the smallest radius of all MT spheres and $K_{max}$ the plane wave cutoff. The valence wave functions inside the MT spheres are expanded up to $l_{max} = 10$, while the charge density was Fourier expanded up to $G_{max} = 12$ (au)$^{-1}$. The MT radii were chosen to be 2.5 Bohr for both Ba and Sn atoms, 2.1 Bohr for Si atoms, and 2.3 Bohr for As atoms. The exchange correlation potential was calculated using the Perdew-Burke-Ernzerhof generalized gradient approximation (PBE-*GGA*).[35] Self-consistency was achieved using 99 $k$-points in the irreducible Brillouin zone (IBZ). The BZ integration was performed using the tetrahedron method and the self-consistent calculations were considered to have converged if the total energy and the charge of the system are stable within $10^{-4}$ Ryd and $10^{-4}$ $e^-$, respectively. Electron localization function (ELF)[36] was calculated

Table 2. Refined Atomic Coordinates and Isotropic Displacement Parameters for $Ba_{13}Si_6Sn_8As_{22}$

| atoms | Wyckoff site | *x* | *y* | *z* | $U_{eq}$ (Å$^2$) |
|---|---|---|---|---|---|
| Ba1 | *16j* | 0.12531 (3) | 0.36680 (3) | 0.58465 (3) | 0.01390 (9) |
| Ba2 | *8i* | 0.16764 (3) | 0.16764 (3) | 0.32488 (5) | 0.01800 (13) |
| Ba3 | *2a* | 0 | 0 | 0 | 0.0420 (4) |
| Si1 | *8i* | 0.41552 (11) | 0.41552 (11) | 0.10009 (17) | 0.0087 (5) |
| Si2 | *4d* | 0 | 1/2 | 1/4 | 0.0090 (7) |
| Sn | *16j* | 0.27221 (3) | 0.45041 (3) | 0.33424 (4) | 0.01409 (10) |
| As1 | *16j* | 0.09239 (4) | 0.39793 (4) | 0.34422 (5) | 0.01351 (14) |
| As2 | *8g* | 0.18681 (6) | 0 | 1/2 | 0.01263 (19) |
| As3 | *8i* | 0.32088 (4) | 0.32088 (4) | 0.19915 (6) | 0.0117 (2) |
| As4 | *8i* | 0.33085 (6) | 0.33085 (6) | 0.47532 (7) | 0.0207 (2) |
| As5 | *4e* | 0 | 0 | 0.28258(10) | 0.0133 (3) |

[a] $U_{eq}$ is defined as one-third of the trace of the orthogonalized $U^{ij}$ tensor.

Table 3. Important Interatomic Distances (Å) in $Ba_{13}Si_6Sn_8As_{22}$

| atom pairs | distances (Å) | atom pairs | distances (Å) |
|---|---|---|---|
| Ba1 − As1 | 3.3235(8) | Ba2 − As1 × 2 | 3.5193(7) |
| As1 | 3.3282(7) | As2 × 2 | 3.4066(5) |
| As1 | 3.5736(7) | As3 | 3.5719(11) |
| As1 | 3.5825(8) | As5 | 3.4817(6) |
| As2 | 3.3777(8) | Ba3 − As4 × 4 | 3.4814(12) |
| As3 | 3.2259(7) | As5 × 2 | 3.8292(14) |
| As4 | 3.3661(8) | | |
| Si1 − As2 × 2 | 2.3525(14) | Sn − As1 × 2 | 2.7169(7) |
| As3 | 2.358(2) | As3 | 2.7146(8) |
| As5 | 2.350(2) | As4 | 2.7158(9) |
| Si2 − As1 × 4 | 2.3679(6) | | |

using the CASTEP code[37] with the ultrasoft pseudopotentials[38] and a plane wave cutoff energy of 330 eV applied.

## RESULTS AND DISCUSSION

**Structure Description.** $Ba_{13}Si_6Sn_8As_{22}$ crystallizes in a new structure type with the tetragonal space group $I\bar{4}2m$ (No. 121). In a brief view, the polyanion structure of $Ba_{13}Si_6Sn_8As_{22}$ can be described as basically composed of $[Si_4As_{10}]$ adamantane-like supertetrahedra and $SiAs_4$ tetrahedra. These units are connected through dimerized $[Sn_2As_4]$ groups to construct a very complex three-dimensional framework and the $Ba^{2+}$ cations are filled into the cavities formed by various As atoms, as shown in Figure 1. The $[Si_4As_{10}]$ cluster consists of four corner-sharing $SiAs_4$ tetrahedra, which are centered by Si1 atoms and slightly distorted with related Si−As bonds ranging from 2.350(2) to 2.358(2) Å. These distances are a little shorter than those of the "discrete" $[SiAs_4]$ tetrahedra formed with Si2 atoms (2.3679(6) Å) and suggest probably stronger Si−As interactions and more localized electron population in $[Si_4As_{10}]$ clusters. In spite of such discrepancies, these Si−As bonds are still in a normal distance range when compared to those silicon-arsenide-based analogues: i.e., 2.36(10) to 2.441(4) Å in $Na_{10}Si_2As_6$,[39] 2.407(5) Å in $Ba_4SiAs_4$,[40] and 2.341(12) to 2.41(5) Å in $Ba_3Si_2As_4$.[41]

The connecting fashion related to these interesting building units is clearly indicated in Figure 2. Each $[Si_4As_{10}]$ supertetrahedral cluster is connected by four $[Sn_2As_4]$ groups through four vertex As3 atoms (in the figure only one is shown for clarity) and then each $[Sn_2As_4]$ group further bridges two "discrete" $SiAs_4$ tetrahedra *via* two As1 atoms. Such a dimerized $[Sn_2As_4]$ structural unit, constructed by two edge-sharing $SnAs_3$ triangular pyramids, is also emphasized in Figure 2. For tin-arsenide-based Zintl phases, various building blocks have been reported such as isolated or edge-sharing $SnAs_4$ tetrahedra in $Na_5SnAs_3$,[42] $K_4Ba_2SnAs_4$,[43] and $A_2SnAs_2$ (A = Cs, Rb),[44] dimerized $[Sn_2As_5]$ units in $Ba_3Sn_4As_6$[28] and $[Sn_2As_6]$ dumbells in $Ba_3Sn_2As_4$.[45] Although such a $[Sn_2As_4]$ unit composed of two edge-sharing $SnAs_3$ triangular pyramids is relatively rare, similar structural fragments have also been observed in $K_6Sn_3As_5$.[46] The Sn−As distances in $Ba_{13}Si_6Sn_8As_{22}$ range from 2.7146(8) to 2.7170(8) Å and are comparable to those reported ternary tin−arsenic-based analogues. For instance, the

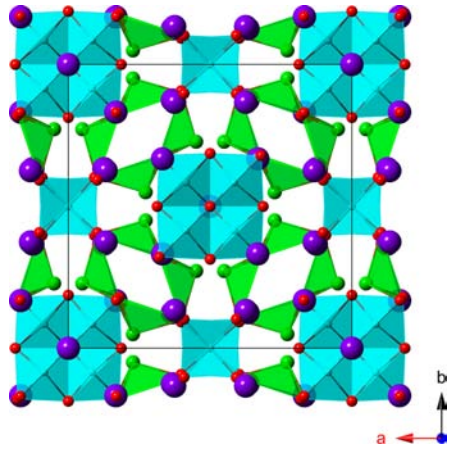


**Figure 1.** Polyhedral representation of the crystal structure of $Ba_{13}Si_6Sn_8As_{22}$, viewed down the *c*-axis. The Ba, Si, Sn, and As atoms are indicated as purple, light blue, green, and red spheres, respectively.

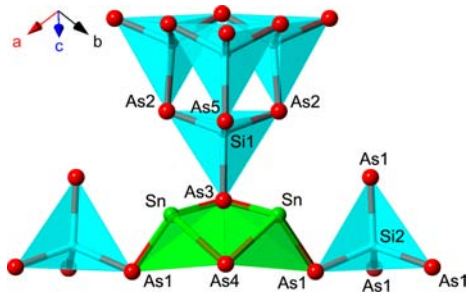


**Figure 2.** View of the polyanion fragment in $Ba_{13}Si_6Sn_8As_{22}$, showing the connecting fashion between the $[Si_4As_{10}]$ supertetrahedral clusters and the $SiAs_4$ tetrahedral units. The $[Sn_2As_4]$ group comprising two edge-sharing $SnAs_3$ triangular pyramids is outlined as well.


dx.doi.org/10.1021/ic402023z | *Inorg. Chem.* 2013, 52, 11836−11842

Sn−As bonding distances vary from 2.7151(2) to 2.7174(3) Å in puckered [SnAs] sheets of KSnAs[47] and from 2.647(2) to 2.727(3) Å in [$Sn_2As_4$] groups of $K_6Sn_3As_5$.[46]

There are three unique Ba cations in the structure and their coordination geometries are very different, as plotted in Figure 3. For Ba1, it resides in a capped octahedron composed of

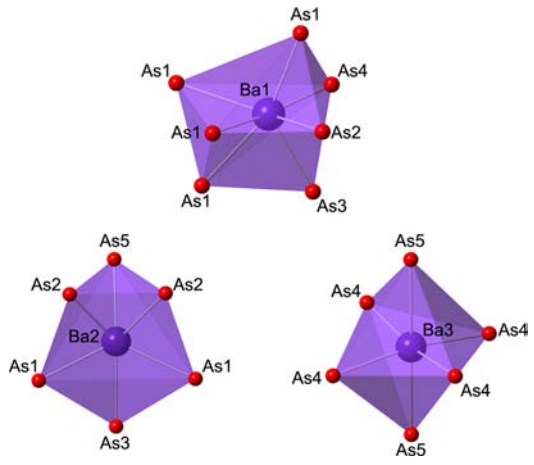


**Figure 3.** Coordination geometry plot for various Ba cations in $Ba_{13}Si_6Sn_8As_{22}$ and related atoms are labeled in graph.

seven As atoms and for Ba2 and Ba3; although they possess the same coordination number, both surrounded by six As atoms, their coordination spheres have distinct differences. The coordination geometry for Ba2 can be described as a distorted trigonal antiprism and for Ba3 a rather distorted $As_6$ octahedron is found instead. Besides the coordination geometries, the related Ba−As distances are significantly different for these barium cations. In the coordination sphere of Ba1, the shortest Ba−As bond has a distance of only 3.2259(7) Å, about 0.25 Å shorter than the longest one. Such a short distance matches well with the sum of the experienced covalent radius for Ba (1.98 Å) and As (1.20 Å).[48] Hence, Ba1 atoms cannot be simply treated as the electron donor or space filler, and its participation in bonding is possibly not neglectable. For the cation Ba2, coordinated by six As atoms, the former bears regular Ba−As distances varying from 3.4817(6) to 3.5719(11) Å, very common for the Ba−As bonds with the octahedral coordination fashion.[49,50] The cation Ba3, with a very distorted octahedral coordination geometry as mentioned above, shall deserve special discussion here. Its coordination sphere consists of four As4 atoms and two As5 atoms. The As4 atoms, though equally far away from the Ba3 center with a normal Ba−As distance of 3.4814(12) Å, are not coplanar and lie in positions obviously off the equatorial plane. The remaining two As5 atoms are very loosely bonded and a large interatomic distance of 3.8292(14) Å is observed for the Ba3−As5 bonds. All these results point to the fact that a rather distorted $As_6$ octahedron is coordinated to the Ba3 cation. Such a special coordination model may result in elongated anisotropic displacement parameters for Ba3, confirmed by the difference Fourier map (Supporting Information) and suggesting the existence of a small positional disorder along the direction parallel to the Ba3−As5 bonds.

**Optical Absorption Spectrum.** The optical absorption spectrum of $Ba_{13}Si_6Sn_8As_{22}$ was calculated from the measured diffuse reflectance spectrum and the results are shown in Figure 4. The data indicates an absorption edge at 0.99 eV, consistent

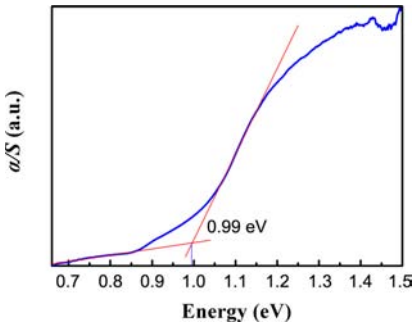


**Figure 4.** Optical absorption spectrum measured on a polycrystalline sample of $Ba_{13}Si_6Sn_8As_{22}$.

with the black color of the crystals. Based on the Tauc plots provided in Figure S4, $Ba_{13}Si_6Sn_8As_{22}$ exhibits an indirect band gap transition lower in energy than the direct band gap transition, which is also consistent with the results of electronic band structure calculations below. The curve also shows a weak band from 0.85 to 1.05 eV, which may be attributed to the absorption of some impurities. Such an optical response should not be related to the absorption of $Ba_3Sn_4As_6$——although this phase may be a possible impurity according to the discussions in the Experimental section, its metallic character will rule out this possibility.[28] Another possible impurity that accounts for such a weak absorption may come from the Si reactant, which is excessively applied in the reactions and can be delivered by the Sn flux (the existence of trace Sn in the sample was confirmed by the TG-DSC measurements below); however, this suspicion is very difficult to verify by the powder XRD patterns since they do not provide any significant evidence.

The existence of a band gap in $Ba_{13}Si_6Sn_8As_{22}$ is reasonable if taking into account the closed-shell electronic configuration of Zintl phases, and comparable values have also been reported for some recently discovered arsenide analogues, i.e., $Cs_8Zn_{18}As_{28}$[18] and $Ca_2CdAs_2$.[21] However, there are also many exceptions that bear near-zero band gaps or even exhibit metallic properties.[28,49] These results reveal that, for arsenide Zintl phases, the electronic band structures can be very complicated and vary significantly with structures and components. To better understand the related physical properties, an in-depth theoretical investigation will be necessary and the results are presented as below.

**Thermal Stability.** Differential thermal analysis (DTA) and thermogravimetry (TG) experiments were performed in order to evaluate the thermal stability of $Ba_{13}Si_6Sn_8As_{22}$, and the results are presented in Figure S3 (Supporting Information). According to the DTA data, there is no significant mass loss observed over the whole measured temperature range. However, in the corresponding DSC curve two obvious endothermic peaks appear at around 500 and 1045 K, respectively. The former, with a relatively small area, should be designated as the melting process of Sn, while the latter could be related to the decomposition of the title compound. This point was demonstrated by the subsequent powder XRD characterization of the decomposing products after TG-DSC experiments (Figure S5 in SI), which indicated that $Ba_{13}Si_6Sn_8As_{22}$ decomposed into $Ba_3Sn_4As_6$ and some uncertain binaries in the high temperature region.

**Electronic Band Structure.** The calculated electronic band structure of $Ba_{13}Si_6Sn_8As_{22}$ is shown in Figure 5 and the results indicate that $Ba_{13}Si_6Sn_8As_{22}$ has a band gap of 0.75 eV. The


dx.doi.org/10.1021/ic402023z | Inorg. Chem. 2013, 52, 11836−11842

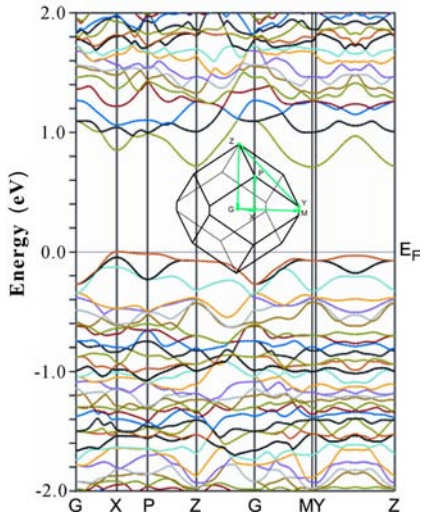


**Figure 5.** Calculated electronic band structure of $Ba_{13}Si_6Sn_8As_{22}$. Inset shows the Brillouin zone of $Ba_{13}Si_6Sn_8As_{22}$ with selected *k*-space directions labeled.

calculated band gap is a little smaller than the measured value due to the GGA approximation, which often leads to underestimated results. The valence band maximum (VBM) and the conduction band minimum (CBM) are located at different *k*-vectors, here *X* and *M* respectively, suggesting that $Ba_{13}Si_6Sn_8As_{22}$ should be an indirect band gap semiconductor.

Based on the total and projected density of states calculated for various constituent atoms in the vicinity of the Fermi level (Figure 6), the conduction and valence bands are generally

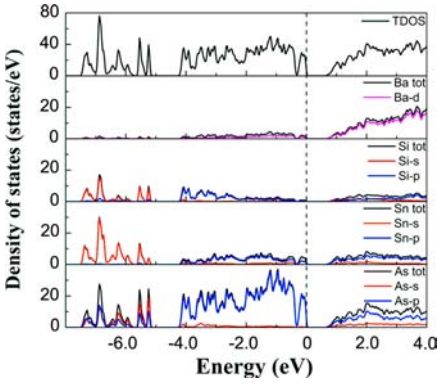


**Figure 6.** Calculated total and projected density of states for various constituent atoms in $Ba_{13}Si_6Sn_8As_{22}$. The Fermi level is selected as the energy reference.

contributed by the 4*p*-orbitals of As, 5*p*-orbitals of Sn, and 5*d*-orbitals of Ba; however, more careful observation reveals that right below the Fermi level, the occupied 4*p*-orbitals of As form a sharp peak and have negligible mixing with Sn or Ba. These results suggest the presence of lone pair electrons on As, which may play an important role in related NLO properties. In addition, the dispersions of the occupied 3*p*-orbitals of Si locate in relatively lower energy levels. This information depicts a picture that Si atoms can be merely viewed as an electron donor and they have minor effects on corresponding physical properties of $Ba_{13}Si_6Sn_8As_{22}$. The differences of the occupied *p*-orbitals between Si and Sn are very obvious if comparing the density of states below the Fermi level: the relatively localized 3*p*-orbitals of Si dominate a narrow energy range from −4.25 to −2.3 eV, which corresponds to the bonding states of Si−As interactions, while for Sn, its 5*p*-states exhibit a very dispersed distribution over a broad range from −4.25 eV to the Fermi level. Such discrepancies can be understood by taking into account their different coordination environments in crystal structure. Since all Si atoms lie in the centers of $As_4$ tetrahedra, strong Si−As covalent bonding interactions can be expected and thus their bonding and antibonding states should have a large energy separation; however, in $SnAs_3$ triangular pyramids each Sn atom is only three-bonded, which allows the presence of electron lone pairs on Sn atoms if assuming the octet rule. This hypothesis was proven by ELF calculations in Figure 7,

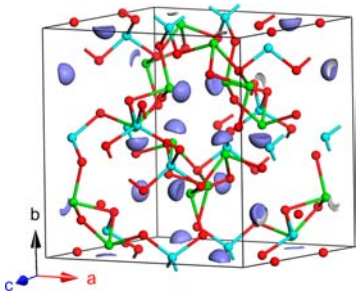


**Figure 7.** Plot of the lone pair electrons on Sn atoms localized by the ELF calculations with CASTEP code using ultrasoft pseudopotentials and a plane-wave expansion of the wave functions. The Si, Sn, and As atoms are indicated as light blue, green, and red spheres, respectively.

which clearly shows the localization of nonbonding electrons on each pyramidally coordinated Sn atom. The ELF calculations also reveal different bonding interactions between Si−As and Sn−As bonds. The former are obviously more covalent with bonding electrons significantly localized between Si and As atoms; however, for the latter they no longer resemble the typical two-center-two-electron covalent bonds with the bonding electrons more delocalized (Figure S6 in SI).

The electronic structure of $Ba_{13}Si_6Sn_8As_{22}$ also raises an interesting question about the electron counting of this compound. By using the Zintl concepts, the charges of three-bonded Sn and four-bonded Si can be assigned as −1 and 0, respectively. Similarly, for the 22 As atoms, 4 occupy the vertex positions of the $[Si_4As_{10}]$ clusters and the remaining 18 bridge 2 triel atoms; thus, the former are three-bonded and should have a zero charge, whereas the latter are all two-bonded and the charge can be designated as −1. Hence, a charge-balanced system $[Ba^{2+}]_{13}[Si^0]_6[Sn^-]_8[As^0]_4[As^-]_{18}$ is the result. Alternatively, the charges of tetrel atoms can be described as $Si^{4+}$ and $Sn^{2+}$, respectively. The divalent $Sn^{2+}$ ions, usually having threefold coordination and a lone pair of electrons, have been seen in references[51] and also proven by the ELF calculations above. The charges of Ba and As atoms can be assumed as 2+ and 3−. This will also lead to an electron precise formulizm of $[Ba^{2+}]_{13}[Si^{4+}]_6[Sn^{2+}]_8[As^{3-}]_{22}$. It should be noted that these two descriptions have no essential differences, since in either case the shared electrons of Si−As or Sn−As bonds are just arbitrarily assigned and should not be viewed as the real life of the electronic structure. What really counts is that both models unambiguously support the localization of electron lone pairs on Sn atoms.


dx.doi.org/10.1021/ic402023z | *Inorg. Chem.* 2013, 52, 11836−11842

## CONCLUSIONS

In conclusion, a new quaternary arsenide Zintl phase $Ba_{13}Si_6Sn_8As_{22}$ has been synthesized by utilizing Sn as the self-flux. Its structure and composition were accurately determined through single-crystal X-ray diffraction and EDX analysis. The polyanionic framework of $Ba_{13}Si_6Sn_8As_{22}$ is built from interesting $[Si_4As_{10}]$ supertetrahedral clusters and $SiAs_4$ tetrahedral units, which are interlinked *via* the $[Sn_2As_4]$ groups comprising two edge-sharing $SnAs_3$ triangular pyramids. Theoretical calculations suggest a small band gap for the compound, proved by the optical absorption spectrum. Based on the calculated electronic band structure and the ELF results, the extensive existence of lone pair electrons on As and Sn atoms is evidential, which may suggest interesting NLO properties combined with its novel polyanion structure.

## ASSOCIATED CONTENT

### Supporting Information

The X-ray crystallographic file in CIF format of the title compound; disordered structure model refined with Ba3 split; the plot of difference Fourier map around the Ba3 atom; elemental analysis on a single crystal of $Ba_{13}Si_6Sn_8As_{22}$ by EDX; powder X-ray diffraction patterns and TG-DSC data of the polycrystalline samples of $Ba_{13}Si_6Sn_8As_{22}$; Tauc plots for $Ba_{13}Si_6Sn_8As_{22}$; ELF analysis illustrating various bonding interactions; powder X-ray diffraction experiments on the decomposition products of $Ba_{13}Si_6Sn_8As_{22}$ after TG-DSC. This material is available free of charge via the Internet at http://pubs.acs.org.

## AUTHOR INFORMATION

### Corresponding Author

*E-mail: shqxia@sdu.edu.cn. Phone: (531) 883-62519, Fax: (531) 883-62519.

### Notes

The authors declare no competing financial interest.

## ACKNOWLEDGMENTS

The authors acknowledge the financial support from the National Natural Science Foundation of China (Grant Nos. 51271098, 51021062, 51272129), the Shandong Provincial Natural Science Foundation (Grant Nos. ZR2010BM003), the Independent Innovation Foundation of Shandong University (IIFSDU), the Program of Introducing Talents of Disciplines to Universities in China (111 program no. b06017) and the 973 Program of the People's Republic of China (Grant Nos. 2010CB630702).

## REFERENCES

(1) Kauzlarich, S. M. *Chemistry, Structure, and Bonding of Zintl Phases and Ions*; VCH Publishers: New York, 1996.
(2) Mills, A. M.; Lam, R.; Ferguson, M. J.; Deakin, L.; Mar, A. *Coord. Chem. Rev.* **2002**, *233*, 207−222.
(3) Papoian, G. A.; Hoffmann, R. *Angew. Chem., Int. Ed.* **2000**, *39*, 2408−2488.
(4) Snyder, G. J.; Toberer, E. S. *Nat. Mater.* **2008**, *7*, 105−114.
(5) Corbett, J. D. *Angew. Chem., Int. Ed.* **2000**, *39*, 670−690.
(6) Xia, S.-Q.; Bobev, S. *J. Am. Chem. Soc.* **2007**, *129*, 4049−4057.
(7) Nomura, T.; Kim, S. W.; Kamihara, Y.; Hirano, M.; Sushko, P. V.; Kato, K.; Takata, M.; Shluger, A. L.; Hosono, H. *Supercond. Sci. Technol.* **2008**, *21*, 125028.
(8) Rotter, M.; Tegel, M.; Johrendt, D. *Phys. Rev. Lett.* **2008**, *101*, 107006.
(9) Wang, X. C.; Liu, Q. Q.; Lv, Y. X.; Gao, W. B.; Yang, L. X.; Yu, R. C.; Li, F. Y.; Jin, C. Q. *Solid State Commun.* **2008**, *148*, 538−540.
(10) Goforth, A. M.; Klavins, P.; Fettinger, J. C.; Kauzlarich, S. M. *Inorg. Chem.* **2008**, *47*, 11048−11056.
(11) Toberer, E. S.; May, A. F.; Snyder, G. J. *Chem. Mater.* **2010**, *22*, 624−634.
(12) Gascoin, F.; Ottensmann, S.; Stark, D.; Haïle, S. M.; Snyder, G. J. *Adv. Funct. Mater.* **2005**, *15*, 1860−1864.
(13) Brown, S. R.; Kauzlarich, S. M.; Gascoin, F.; Snyder, G. J. *Chem. Mater.* **2006**, *18*, 1873−1877.
(14) Zevalkink, A.; Zeier, W. G.; Pomrehn, G.; Schechtel, E.; Tremel, W.; Snyder, G. J. *Energy Environ. Sci.* **2012**, *5*, 9121−9128.
(15) Stoyko, S. S.; Khatun, M.; Mar, A. *Inorg. Chem.* **2012**, *51*, 2621−2628.
(16) Stoyko, S. S.; Mar, A. *Inorg. Chem.* **2011**, *50*, 11152−11161.
(17) Khatun, M.; Stoyko, S. S.; Mar, A. *Inorg. Chem.* **2013**, *52*, 3148−3158.
(18) He, H.; Zevalkink, A.; Gibbs, Z. M.; Snyder, G. J.; Bobev, S. *Chem. Mater.* **2012**, *24*, 3596−3603.
(19) He, H.; Tyson, C.; Bobev, S. *Inorg. Chem.* **2011**, *50*, 8375−8383.
(20) Marder, S. R.; Sohn, J. E.; Stucky, G. D. *Materials for Nonlinear Optics: Chemical Perspectives*; American Chemical Society: Washington, DC, 1991.
(21) Wang, J.; Yang, M.; Pan, M.-Y.; Xia, S.-Q.; Tao, X.-T.; He, H.; Darone, G.; Bobev, S. *Inorg. Chem.* **2011**, *50*, 8020−8027.
(22) Yu, P.; Zhou, L.; Chen, L. *J. Am. Chem. Soc.* **2012**, *134*, 2227−2235.
(23) Eisenmann, B.; Schäufer, H. *Z. Anorg. Allg. Chem.* **1982**, *491*, 67−72.
(24) Huang, F. Q.; Deng, B.; Ellis, D. E.; Ibers, J. A. *J. Solid State Chem.* **2005**, *178*, 2128−2132.
(25) Eisenmann, B.; Hofmann, A. *Z. Kristallogr.* **1991**, *197*, 171−172.
(26) Eisenmann, B.; Hofmann, A. *Z. Kristallogr.* **1991**, *195*, 318−319.
(27) Asbrand, M.; Eisenmann, B. *Z. Naturforsch., B: Chem. Sci.* **1993**, *48*, 452−456.
(28) Lam, R.; Mar, A. *Solid State Sci.* **2001**, *3*, 503−512.
(29) *Bruker APEX2*; Bruker AXS Inc.; Madison, WI, 2005.
(30) Sheldrick, G. M. *SHELXTL*; University of Göttingen, Göttingen, Germany, 2001.
(31) Kortüm, G.; Lohr, J. E. *Reflectance Spectroscopy: principles, methods, applications*; Springer-Verlag: New York, 1969.
(32) Madsen, G. K. H.; Blaha, P.; Schwarz, K.; Sjostedt, E.; Nordstrom, L. *Phys. Rev. B* **2001**, *64*, 195134.
(33) Schwarz, K.; Blaha, P.; Madsen, G. K. H. *Comput. Phys. Commun.* **2002**, *147*, 71−76.
(34) Blaha, P.; Schwarz, K.; Madsen, G. K. H.; Kvasnicka, D.; Luitz, J. *WIEN2k, An Augmented Plane Wave + Local Orbitals Program for Calculating Crystal Properties*; Technische Universität: Vienna, Austria, 2001.
(35) Perdew, J. P.; Burke, S.; Ernzerhof, M. *Phys. Rev. Lett.* **1996**, *77*, 3865−3868.
(36) Silvi, B.; Savin, A. *Nature* **1994**, *371*, 683−686.
(37) Segall, M.; Linda, P.; Probert, M.; Pickard, C.; Hasnip, P.; Clark, S.; Payne, M. *J. Phys.: Condens. Matter* **2002**, *14*, 2717−2744.
(38) Vanderbilt, D. *Phys. Rev. B* **1990**, *41*, 7892−7895.
(39) Eisenmann, B.; Klein, J. *Z. Kristallogr.* **1991**, *197*, 267−268.
(40) Eisenmann, B.; Jordan, H.; Schäfer, H. *Angew. Chem. Int. Engl.* **1981**, *20*, 197−198.
(41) Eisenmann, B.; Jordan, H.; Schäfer, H. *Z. Naturforsch., B: Chem. Sci.* **1982**, *37*, 1564.
(42) Eisenmann, B.; Klein, J. *Z. Kristallogr.* **1991**, *196*, 213−229.
(43) Eisenmann, B.; Röβler, U. *Z. Anorg. Allg. Chem.* **2000**, *626*, 1373−1379.
(44) Eisenmann, B.; Klein, J. *J. Less Common Met.* **1991**, *175*, 109−117.
(45) Eisenmann, B.; Jordan, H.; Schäfer, H. *Z. Naturforsch., Teil B: Anorg. Chem.* **1984**, *39*, 1151−1153.
(46) Klein, J.; Eisenmann, B. *Mater. Res. Bull.* **1988**, *23*, 587−594.
(47) Lii, K.; Haushalter, R. C. *J. Solid State Chem.* **1987**, *67*, 374−378.

(48) Sanderson, R. T. *Inorganic Chemistry*; Reinhold: New York, 1967.
(49) Mathieu, J.; Achey, R.; Park, J.-H.; Purcell, K. M.; Tozer, S. W.; Latturner, S. E. *Chem. Mater.* **2008**, *20*, 5675−5681.
(50) He, H.; Tyson, C.; Saito, M.; Bobev, S. *J. Solid State Chem.* **2012**, *188*, 59−65.
(51) Chernaya, V. V.; Mitiaev, A. S.; Chizhov, P. S.; Dikarev, E. V.; Shpanchenko, R. V.; Antipov, E. V.; Korolenko, M. V.; Fabritchnyi, P. B. *Chem. Mater.* **2005**, *17*, 284−290.